RESPONSE OF SINGLE LMFBR TYPE HEXCANS TO STATIC AND DYNAMIC LOADS—SOME EXPERIMENTS AND ANALYSIS

J.E. ASH, T.J. MARCINIAK

Reactor Analysis and Safety Division, Argonne National Laboratory, Argonne, Illinois 60439, U.S.A.

D.J. CAGLIOSTRO

Stanford Research Institute, Menlo Park, California 94025, U.S.A.

SUMMARY

Determination of the structural response of Liquid Metal Fast Breeder Reactor (LMFBR) subassembly ducts to postulated local energy releases is a complex problem. The factors entering into the problem include (a) the geometry of the structure, (b) uncertainty in the definition of the energy release rate and subsequent pressure pulse, (c) uncertainty of material properties under reactor operating conditions, and (d) difficulty of performing either out-of-pile, or in-pile experiments to verify and extend analysis. In order to minimize the uncertainties involved in predicting the structural response, an analytical and experimental effort has been undertaken to devise computational techniques valid over a wide range of postulated events and material properties. The effort centers mainly upon an out-of-pile experimental program which has been devised and is being carried out to verify and extend finite-element computer codes designed to evaluate duct response under reactor operating conditions.

In order to verify the finite-element codes, a series of experiments has been performed under quasi-static and dynamic conditions. Since for moderate deflections, end effects influence the axial deformation profile over only a limited distance, it was not necessary to use full length subassembly ducts in the experiments. Preliminary static tests demonstrated that for the range of deformations expected in a single subassembly prior to failure, a shortened duct section of only 30.48 cm in length was sufficient to provide a central test section over which axially uniform conditions prevailed. As a result, the deformation over the uniform range corresponds to two-dimensional plane-strain conditions, and a two-dimensional computer code can be applied for the analysis. Additional static tests were then performed using a series of Type 316 stainless steel hexcan specimens in which the ductility was varied from a fully annealed specimen to a brittle specimen with a hardness corresponding to 50% cold working. Each experiment was fully instrumented to measure the internal pressure loading distribution and the corresponding strains and displacements at critical points such as the midflat region of maximum deflection and the duct corners where failure was expected.

Dynamic tests of hexcans were also performed using a pressure-time source designed to duplicate a postulated local event. The local event simulated was the failure, after some period of operation, of misloaded, overenriched fuel pins. The fuel pin failure was postulated to result in the release of molten fuel into several subassembly subchannels. The resulting pressure pulse had the general characteristics of a 1 msec risetime to a peak of about 100 bar, with a total pulse width of about 5 msec. Dynamic pulse loading experiments were then performed, in which the pressure pulse plus midflat and corner strains and displacements were measured. Along with the extensive test instrumentation, the material properties were also carefully determined for each specimen. An accurate determination of the material properties in each case was necessary because of the high sensitivity of the hexcan response to the elastic modulus, the yield point and the plastic flow stress-strain relationship.

It is felt that, although these experiments are of a relatively simple nature, they can go a long way in explaining some of the phenomenology of hexagonal duct response to dynamic loading. From this knowledge confidence can be gained in analysis applied to end-of-life conditions.

1. Introduction

The problem of determining the response of Liquid Metal Fast Breeder Reactor (LMFBR) fuel subassemblies to local accidental events and resultant possible propagation of damage to surrounding subassemblies or control-rod positions is difficult to approach from either an experimental or purely analytical point of view. Factors which must be considered in reaching a solution include: (i) definition of subassembly local accidents which may result in damage both to the accident subassembly and its surroundings; (ii) definition of subassembly-duct material properties at end-of-life under reactor operating or accident conditions; (iii) geometry of the subassembly structure including intersubassembly coolant and surrounding subassemblies.

The definition of local subassembly accidents poses one of the most difficult areas to resolve since a wide range of initiating conditions can be postulated followed by various sequences. The pressure pulses may well range from those expected when one or more end-of-life fuel pins fail, releasing high-pressure fission gas, a type of event with a relatively high probability of occurrence, to a hypothetical event such as a full subassembly blockage of coolant with a resultant fuel (or steel) and coolant interaction, and vapor explosion. The latter event is of very low probability, however, because current reactor designs preclude subassembly blockages, and current understanding of the fuel-coolant-interaction problem indicates that this event should not occur [1]. The intensive studies underway attempting to describe realistic accident sequences should lead to the future definition of realistic pressure-time sources for use in subassembly-damage evaluation. Furthermore, future improvements in the description of the material properties of irradiated subassembly materials should be expected. At present the mechanical material properties, such as ductility, yield strength, and ultimate strength, are nominally known and may be subject to significant variations in specific cases.

Given the uncertainties in defining the pressure pulses and material properties of subassembly ducts, an experimental effort to determine hexcan response to local accidents is difficult to define. The approach used here to describe hexcan response to local events is first to develop reasonable analytical tools and then to devise experiments which can be used to verify, and where necessary, modify and extend the computer codes and analysis.

The main purpose of the experimental effort described here is to perform well-defined and instrumented experiments to provide sufficient data to support the development of the STRAW computer code [2] underway at Argonne National Laboratory. In its current version, STRAW is a two-dimensional code which takes into account the accident subassembly, the intersubassembly coolant, and the surrounding one or two rows of subassemblies, including some representation of the subassembly internals. The experimental program is designed to verify the calculational models which describe the subassembly response. First, quasi-static experiments were performed to define the gross response of subassemblies to internal and external pressures. Then dynamic tests were performed on single hexcans under pressure-pulse loadings using a calibrated and verified pressure-time source. Later extensions of the experimental effort may include subassembly-cluster tests to evaluate subassembly-to-subassembly damage-propagation phenomena. Subassembly ducts having LMFBR hexcan dimensions and materials are being used in the experiments, but various degrees of cold working are used to test the computations for lower-ductility materials. It was found desirable that the

material properties be uniform throughout the hexcan. Uniformity was achieved by careful annealing. However, since an irradiated hexcan has a much lower ductility, code verification for the more brittle material is made possible by controlling the manufacturing process to produce a duct with fairly uniform cold working (50%) properties.

After verification and possible modification of the codes to correlate with the experiments, the codes will be applied to predict actual in-reactor subassembly response to accidental events. By this means, the customary reliance upon out-of-pile experiments to bound the energy source will be avoided. The overall program sequence and approach to the evaluation of in-reactor events is depicted in fig. 1.

2. Related Experimental Studies of the Mechanical Response of Core Subassemblies

This paper describes the current experimental study of a single out-of-pile subassembly hexagonal wrapper. However, it should be pointed out that other closely related subassembly-damage-propagation experimental programs have been undertaken. To see where these studies fit into the context of core accident mechanics, several full-scale experiments will be briefly discussed.

Full-scale testing of subassembly clusters is motivated by the fact that a complete prediction of the events following an accidental fuel-pin failure or local cooling disturbance within a core assembly is beyond the present state of knowledge. It is necessary to understand the mechanical response of the subassembly structure in order to describe the sequence of events following a possible local subassembly accident. These events, which include the hydrodynamic response of the coolant, heat transfer, thermal loading, and material changes, depend upon the boundary conditions of the deforming mechanical geometry. To demonstrate that the mechanical damage will not lead to an excursion, nor make the shut-off system inoperable, full-scale model test programs have been initiated for the British PFR and German SNR core configurations using a very conservative pressure-time source based upon a subassembly blockage and meltdown accident.

2.1 The PFR Tests [3]

In the PFR test program, a cluster of 61 subassemblies was subjected to a very energetic pressure pulse of long duration (10 msec). The pulse was generated by controlled burning of a propellent explosive in a centrally located subassembly. The subassembly wall was artificially weakened to reproduce the effect of duct wall overheating during the postulated accident event. The surrounding simulated subassemblies suffered extensive permanent deformations. In spite of the apparent damage, the asserted conclusions were that the outer control rods would probably function and that fuel pins in the surrounding subassemblies would probably remain intact. Questions were raised about the effect of possible core springback upon recompaction reactivity rates, and a repetition of the experiments with improved core constraint simulation was recommended.

2.2 The SNR Tests [4]

A somewhat similar testing of the SNR core using the same pressure-pulse generator as for the PFR test program is underway. In the preliminary reported test results, the pressurized subassembly ruptured at a peak pressure of only 525 psi. No permanent deformations of the surrounding subassemblies were observed. Auxiliary tests using a drop tower were made to determine the stiffening influence of internal fuel pins against wrapper deformations by external loads.

2.3 EBR-II Tests [5]

The tests mentioned above are of an upper-bound nature for the gross effects of a sequence of complex structural interactions. Questions of subassembly and fuel-pin failure propagation are not completely resolved, and require further systemmatic study of the details of the changes in the structural geometry in order to support a logical analysis of the accident sequence. To establish the fundamental relationships between loading and response, experiments were performed at Argonne National Laboratory to determine the response of an isolated EBR-II subassembly to simulated fuel-pin-failure loadings. Analysis [6] of these experiments and correlation with a finite-element structural code demonstrated that good predictions of elastic-plastic deformations for a single out-of-pile subassembly hexcan-wrapper can be achieved, providing that the material properties and loading conditions can be well-defined.

3. The Finite-element Structural Code

The basic structural computer code used in the analysis of the hexcan deformations was STRAW, a nonlinear, transient, finite-element program. The code is two-dimensional so that repeated computational trials to study parameter changes can be quickly and economically run. The range under which the two-dimensional code is applicable was indicated by comparisons with a full three-dimensional code (SADCAT) [7]. To reproduce two-dimensional conditions in the experiments, the test rig was designed to provide a region midway between the ends of the hexcan over which conditions are uniform along the length and plane-strain conditions hold. The STRAW code uses flexural beam elements and an explicit forward integration in time. The code is limited to small strains, but large rotations and deflections are permitted through the use of convected coordinates.

4. Material Properties

Of particular importance for prediction of hexcan deflections under a specified loading is the description of the material properties as input data to the code. Stress concentrations in the corners of the hexcan will cause plastic flow for even relatively small deflections of the midflat. This necessitates an accurate knowledge of the yield point, for the plastic hinge effect causes the midflat deflection to increase sharply when the elastic limit is exceeded. Because of the sensitivity of deflection to the plastic-flow material properties, the stress-strain relationship cannot be linearized in the yield region.

A stress reversal in the outer layer at the corner, shown in fig. 2, gives rise to a further difficulty in the material description. The material is first compressed until plastic flow and strain-hardening take place. With further deflection, the strain direction reverses, and elastic tensile straining proceeds until yielding in tension occurs. The new tensile yield point depends upon the earlier compressive strain-hardening effect. An example path of possible stress-strain states is shown in fig. 3. Precisely where to expect the new yield point is not known. There are several theories for the strain-hardening effect. For the conventional uniaxial stress-strain diagram the "kinematic hardening" effect assumes an unchanging magnitude for the elastic range; "fixed hardening" assumes an invariant yield stress; and "isotropic hardening" assumes the elastic range is symmetric about the zero stress point. The sample computation shown in fig. 3 illustrates the possible importance of the choice of models. The isotropic model is stiffer, and for the example shown in fig. 3, the isotropic assumption indicates that the hexcan would sustain a pressure of

2000 psi. However, under the assumption of kinematic hardening the tensile yield stress is lowered and the hexcan cannot sustain the same pressure of 2000 psi, but expands out to failure. Based upon indications from other experiments [8], the correlations in this study assume the yield lies between the fixed and kinematic values.

Another source of some difficulty for the correlation of the computations with the test results is that the two-dimensional deformation of the hexcan section remote from end effects is in a plane-strain mode. Axial displacements are constrained. Hence, the flexural beam elements in the core are in a biaxial state of stress. The stress-strain data are from uniaxial tests and must be corrected to apply to the plane-strain problem. The von Mises yield ellipse is used in this approximation. The most direct correction is for the isotropic hardening model, which ignores the Bauschinger effect, and the yield ellipse simply enlarges without translation (in the principal stress space). For kinematic hardening, the yield ellipse is translated but without change of size. For yield points between these extremes, the yield surface both changes size and is translated in the principal stress diagram.

4.1 Determination of the Stress-Strain Relationship

The determination of the stress-strain properties of the test hexcan material will be explained, as the description of the material properties is crucial to the correlation of the code computations with the experimental results. Since the yield point is altered in fabricating the hexagonal shape, a tensile test specimen was taken directly from each sample experimental duct. The wall thickness limits the size of the specimen to a rectangular area of only 0.03 sq in. The gage length of the specimen, shown in fig. 4, is 1 in., and the nonuniform strain distributions resulting from the onset of necking near the ultimate point (u) (see figs. 4 and 5) makes direct strain measurements unreliable.

A method was used in which the plastic flow curve from the proportional limit (p) to the failure point (f) was constructed without direct strain measurements. A power law expression was assumed between the proportional limit and the ultimate point:

$$\sigma = B\varepsilon^{m} , \qquad (1)$$

From the ultimate point out to fracture, a hyperbolic-sine law was assumed:

$$\varepsilon = \varepsilon_{o} + b \sinh(\sigma/\sigma_{c}) , \qquad (2)$$

These laws were found [9] to fit the stainless steel types used in the experiments reasonably well.

From the strip-chart output of the tensile test machine, the only data used are the readily identifiable loads at the proportional limit (p), the maximum load at the ultimate point (u), and at failure (f). The Young's modulus determined in a separate test is relatively independent of the hexcan-forming process, and is used to determine the true-stress and true-strain point (σ_p, ε_p) for the proportional-limit load. The stability condition for necking applied to eq. (1) determines the equation for the exponent m :

$$\frac{(\sigma_u)_e}{\sigma_p} \exp(m) = (m/\varepsilon_p)^{m} , \qquad (3)$$

The ultimate engineering stress $(\sigma_u)_e$ is the maximum load/original area. The value of m is the true strain at the ultimate point (u). For example, the average value of m based upon eight test samples from the annealed can is 0.216, and the corresponding true ultimate stress is 102 ksi. From the now-determined proportional limit and ultimate points, the coefficient B is the slope of the straight line in the log-log plot shown in fig. 5.

The true strain at failure (f) is derived from the measured reduced cross-section area of the fractured specimen. The fracture point lies above the straight line in the log-log plot, and the plastic flow curve in the range between (u) and (f) is fitted to eq. (2), using the point and slope at (u) and point (f) to determine the unknown coefficients ε_o, b, and σ_c.

The straight line is close to the tangent line drawn from (u). For the less ductile 20% and 50% cold-worked samples, the plastic-flow curve from (u) to (f) is very closely approximated by the tangent line from (u).

5. Description of Experiments Using Full-size LMFBR Hexcans

Several experiments have been performed with a concentration on static pressurization of subassembly hexcans. The main reasons for this approach were to determine the gross response of hexcans to static internal pressurization, and to provide reliable pressure, deflection, and strain measurements. Along with these experiments the material properties of the hexcans were determined with particular emphasis on the true stress-engineering strain and the diamond-point hardness along the hexcan flat. This last was considered important since it is desirable to maintain uniform properties in the hexcan, and data gathered previously with some subassembly ducts showed cold-working gradients which affected hexcan deflections significantly.

The apparatus used in both the static and dynamic experiments is shown in fig. 6. The 1-ft-long hexcan was welded to rigid end rings and bolted to thick end plates. In order to restrict end motions during the tests, twelve 1-in.-dia bolts were arranged around the edge of the thick plate. The cross-sectional area of the bolts was such that the end motion was negligible for internal pressurizations up to about 3000 psi. During each test the internal pressure was measured along with midflat and corner deflections. The deflections were measured with sensitive linear potentiometers. Strains were measured in the midflat region in both the axial and circumferential direction. Typical instrumentation is shown in fig. 7.

In order to show that a hexcan with a length of 12 in. was sufficiently long to provide plane-strain conditions with a negligible amount of end effects, a hexcan with a length of 24 in. was also tested. The material properties of each hexcan were those of solution-annealed type 316 stainless steel. The results of these tests are shown in fig. 8. It can be seen that the midflat deflections measured at the midplane of the 12-in. long hexcan matched very well with the 24-in.-long hexcan data. This demonstrates that the 1-ft length is sufficient so that end effects do not significantly influence the correlation of test data at the midplane.

6. Comparisons of Experiments with Analysis

Before attempting to analyze the dynamic response to impulsive pressure loads, correlations were established for the more basic case of hydrostatic or slowly increasing quasi-static pressurization of EBR-II and prototype-sized LMFBR hexcans. Comparisons of computed midflat deflections for EBR-II hexcans with test data are shown in fig. 9 for annealed type 304 and cold worked (20%) type 316 stainless steel hexcans. Preliminary computations, based upon the assumption of a fully annealed can, predicted a midflat deflection at 300 psi of 170 mils, too large by a factor of 2.5 compared to the experimental result. The reason, as revealed by diamond-point-hardness tests, was that residual cold working of up to 25% remained in the corner regions. The effect of the cold working is to raise the yield point

significantly as shown in fig. 10. With the corrected hardness gradient in the corner region, the good correlation shown in fig. 9 resulted. A more accurate description, rather than a straight-line representation, of the nonlinear plastic stress-strain relation after yield gives a further improved correlation.

The material properties were maintained more nearly uniform in later experiments with the full-size LMFBR subassembly. Correlation with experiments in fig. 11 shows the strong influence of ductility upon the maximum deflections. The annealed can expanded out to a nearly circular shape before rupturing. Two deformation regimes are identified in fig. 12. At lower pressures, the deflection mode corresponds to a bending beam with fixed ends; at higher pressures, the can expands out to a circular shape and deforms uniformly in a "hoop stress" mode. The initial deformation is elastic and the pressure vs deflection curve is linear; the slope abruptly changes when the corner yields plastically and the deflection rate rapidly increases with pressure. Under further pressurization, the response again stiffens when the circular hoop-stress mode dominates. Finally, a point is reached where further pressurization cannot be sustained because of a combination of plastic flow, decreasing wall thickness, and increasing projected area over which the pressure is exerted.

The dynamic response of the hexcan to a pressure pulse is compared in fig. 12 to the response under a quasi-static pressurization. At the same pressure, the dynamic deflection lags behind the hydrostatic deflection due to inertial resistance. However, as the peak of the pressure pulse is reached, inertia causes an overshoot in the deflection. These dynamic inertial effects can exert a strong influence upon the final deformation, as is illustrated in fig. 13. For a 1200-psi pressurization at a rise time of 0.5 msec, the peak midflat deflection (280 mils) occurs at 0.6 msec, shortly after the peak pressure is reached. This is an expected response behavior. However, a qualitatively different response behavior was computed when the pressurization was increased to 2000 psi for the same rise time. The expected overshoot appeared with a peak of 360 mils, a peak above the hydrostatic deflection (320 mils), but the return to this hydrostatic position was abruptly stopped, and a further jump in the deflection advanced to a final permanent deformation of 500 mils. This apparently anomalous response behavior is caused by the plastic tensile flow, permitting easy extension, while compressive strain is strongly resisted by the large elastic modulus. Consequently, the deflection occurs in a series of alternating steps in which outward motion of the midflat accompanied by a relatively stationary corner is followed by an outward motion of the corner while the midflat region holds stationary.

7. Conclusions

An experimental program has been initiated to determine the response of LMFBR-type subassemblies to local subassembly accidents. The approach taken in this program is to perform well-defined experiments in which pressures, deflections, and strains can be measured. An effort is also being made to determine material properties of the hexcans and to assure that the material properties are uniform throughout a specimen. Results from the tests are then compared with computer-code calculations in order to check the validity of the analysis and perhaps modify models for more meaningful correlations. The codes then will be used to calculate the response of subassembly ducts under in-reactor accident conditions.

Preliminary comparisons to date show reasonable agreement between calculations and experimental results for annealed and cold worked type 316 stainless steel ducts under static internal-loading conditions. These tests and comparisons were helpful in gaining a knowledge of the way in which hexcans distort under internal pressures. Possibly the tests can be used to extrapolate directly results from tests in which the rise time of the pulse is significantly longer than the natural period of the hexcan. Some understanding too has been gained from dynamic calculations concerning the behavior of subassembly ducts. Further comparisons with dynamic test results will be performed.

Future work will be concerned with testing ducts with material properties more closely approximating those of end-of-life ducts. Although these materials will have low ductility and a yield and ultimate strength approximating end-of-life ducts, they are not intended to be a strict simulant. The purpose is to check the modeling in the computer code using material properties more closely approximating those expected under reactor operating conditions. Propagation phenomena and the effect of intersubassembly coupling in damage propagation will also be investigated.

References

[1] FAUSKE, H. K., "On the Mechanism of Uranium Dioxide-Sodium Explosive Interactions," Nuclear Science and Engineering, 51, pp. 95-101 (1973).

[2] KENNEDY, J. M., "Nonlinear Dynamic Response of Reactor Core Subassemblies," ANL-8065 (January, 1974).

[3] DENNY, P. H., REES, N. J. M.,WARREN, G. R., "An Empirical Study of the Effects of a Simulated Sodium Coolant Vapor Explosion in a Subassembly of the PFR Core Structure," 2nd Intl. Conf. on SMiRT, Paper E 1/7.

[4] GAST, K., LIEBE, R., WILL, H., ZEHLEIN, H., REES, N. J. M., and WARREN, G. R., "Simulated Vapor Explosion Experiments and Dynamic Elasto-plastic Response of SNR Core," Proc. Fast Reactor Safety Mtg., CONF-740401-P2 (April, 1974).

[5] KOENIG, J. F., "Pressure Tests of Hexagonal Cans," ANL-RDP-6 (June, 1972).

[6] ASH, J. E., "Analysis of Hexcan Deformations and Some Comparisons with Out-of-Pile EBR-II Subassembly Duct Experiments," ANL-8154 (December, 1974).

[7] BELYTSCHKO, T. and MARCHERTAS, A. H., "Nonlinear Finite-Element Method for Plates and its Application to Dynamic Response of Reactor Subassemblies," Trans. ASME, Vol 96, Series J, No. 4, pp. 251-257 (November, 1974).

[8] MENDELSON, A., Plasticity: Theory and Application, Macmillan (1968).

[9] DIERCKS, D. R. and BURKE, W. F., "Elevated-Temperature True Stress-True Strain Tensile Behavior of AISI Type 304 Stainless Steel," ASME Pressure Vessel and Piping Conf., Miami Beach (1974).

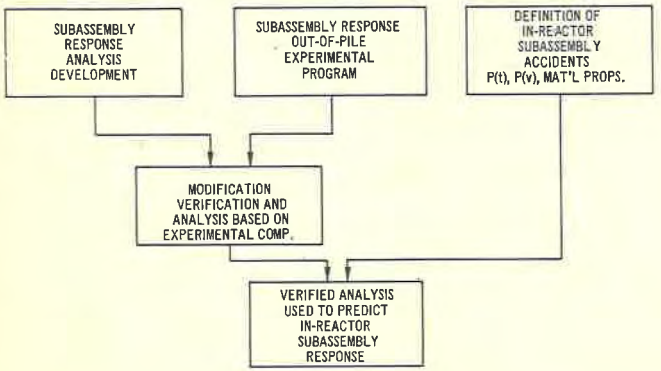

Figure 1 Development of Predictive Analysis Method for Subassembly Response

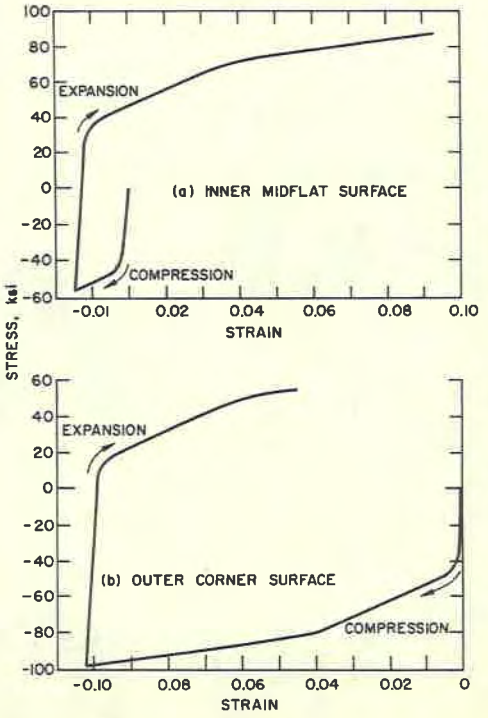

Figure 2 Examples of Stress Reversals at Outer Corner Surface and Inner Midflat Surface for Annealed, Room Temperature, LMFBR Type Hexcans

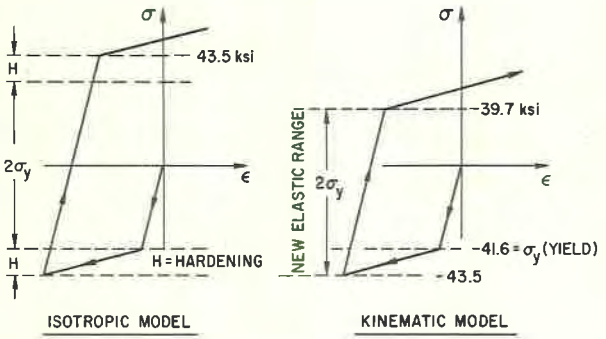

Figure 3 Comparison of Stress-strain States for Isotropic and Kinematic Hardening

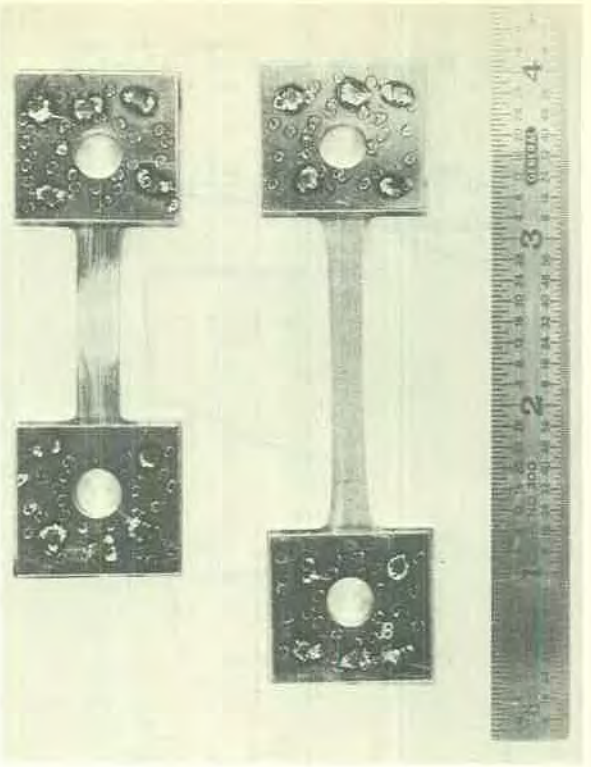

Figure 4 Annealed Type 316 Stainless Steel Tensile Specimens Before and After Testing

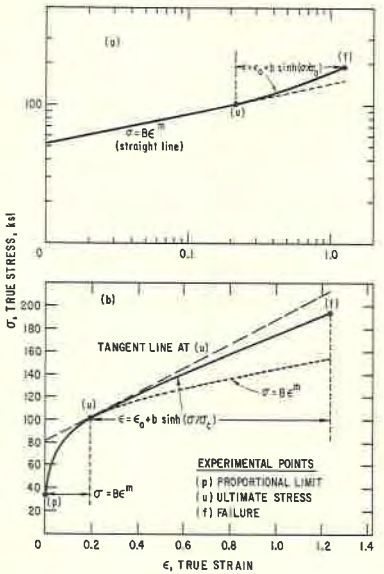

Figure 5 Empirically Fitted Stress-strain Relation for Annealed Type 316 Stainless Steel

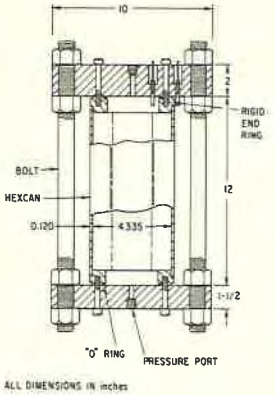

Figure 6 Schematic of Apparatus Used for Single Hexcan Tests

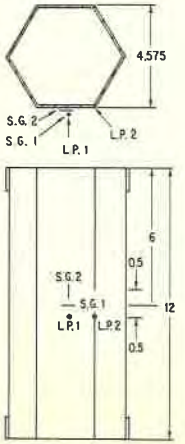

Figure 7 Typical Instrumentation Used for a Single Hexcan Test

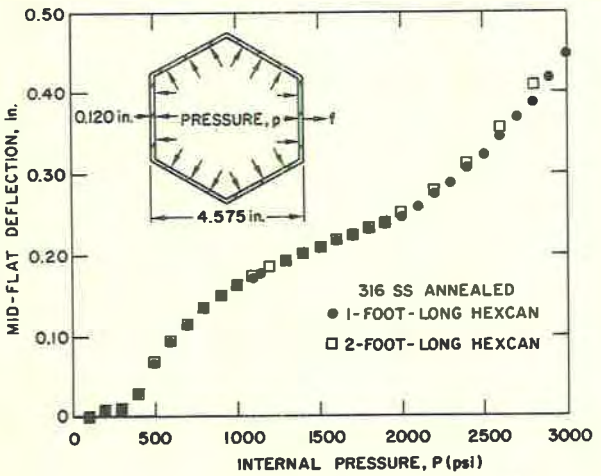

Figure 8 End Effects in Static Loading: Midflat Deflection vs Internal Pressure at Midsection

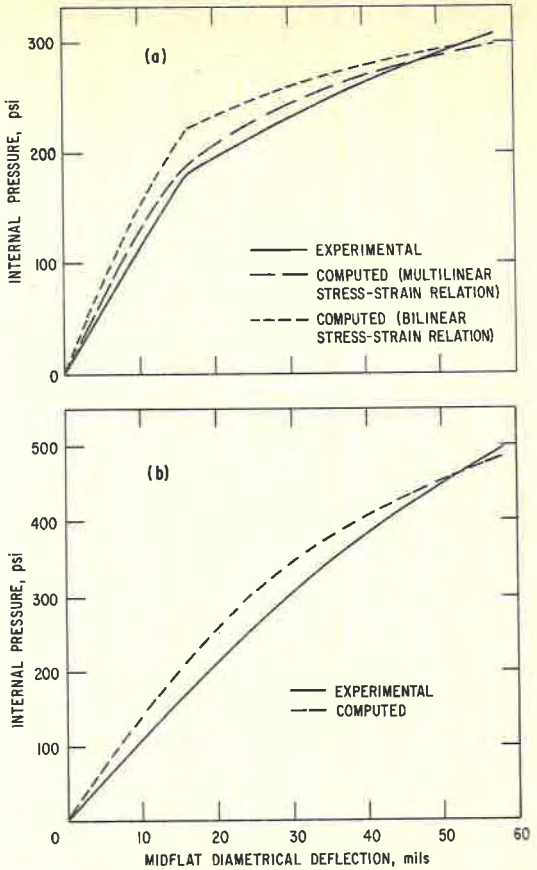

Figure 9 Comparisons of Computed with Experimental Midflat Deflections of Pressurized EBR-II Hexcans

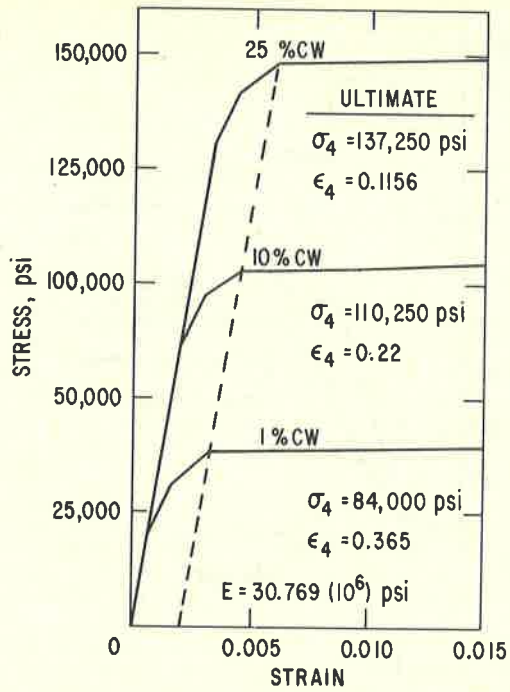

Figure 10 Effect of Cold Work Upon the Stress-strain Properties of Type 316 Stainless Steel

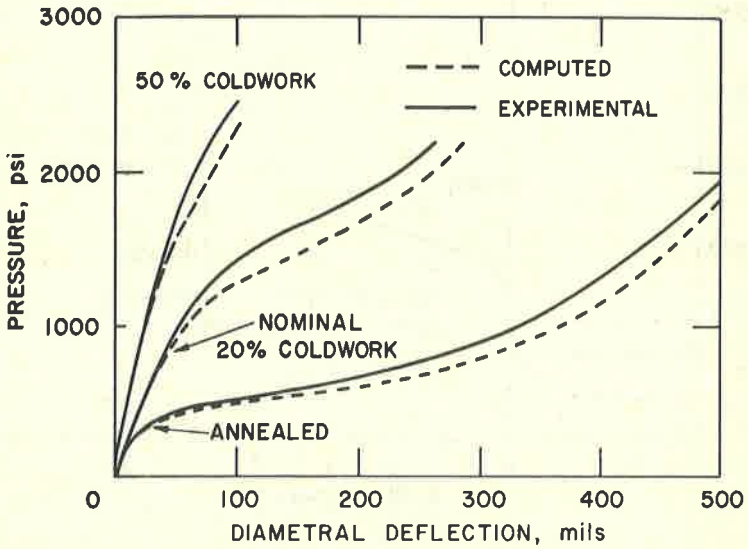

Figure 11 Comparison of Computed with Experimental Midflat Deflections for Pressurized LMFBR Hexcans

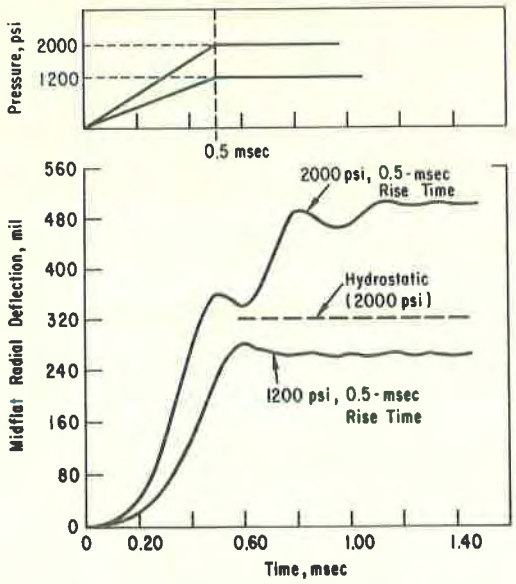

Figure 12 Midflat Deflections for Annealed Type 316 Stainless Steel LMFBR Hexcans Under Static and Dynamic Loads

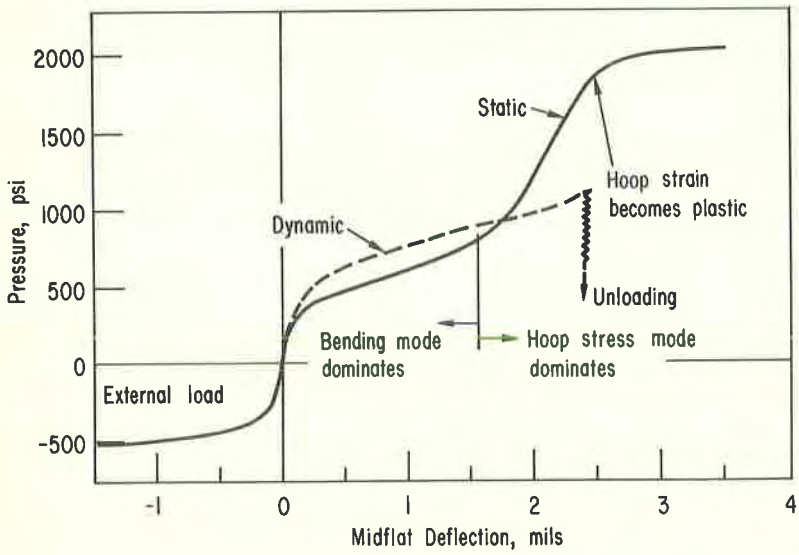

Figure 13 Midflat Radial Deflection Showing Dynamic Overshoot due to Plastic Flow at Internal Pressurization of 2000 psi